DMD Fast Forward. Published on April 2, 2019 as DOI: 10.1124/dmd.118.085605
This article has not been copyedited and formatted. The final version may differ from this version.

TITLE:

Prediction of human nonlinear pharmacokinetics of a new Bcl-2 inhibitor using PBPK modelling and interspecies extrapolation strategy

AUTHORS:

PIERRILLAS Philippe, HENIN Emilie, BALL Kathryn, OGIER Julien, AMIEL Magali, KRAUS-BERTHIER Laurence, CHENEL Marylore, BOUZOM François, TOD Michel

AFFILIATIONS:

EMR 3738, Ciblage Thérapeutique en Oncologie, Faculté de Médecine et de Maïeutique Lyon-Sud Charles Mérieux, Université Claude Bernard Lyon 1, 69600 Oullins, France. (P.P, E.H, M.T)

Pharmacie Hôpital de la Croix Rousse, Hospices Civils de Lyon, Lyon, France. (M.T)

Centre de Pharmacocinétique et Métabolisme, Technologie Servier, Orléans, France. (P.P, F.B)

Clinical Pharmacokinetics and Pharmacometrics Division, Servier, Suresnes, France. (K.B, J.O, M.A, M.C)

Institut de Recherches Internationales Servier, Oncology R&D Unit, Suresnes, France. (L.K-B)

CURRENT AFFILIATIONS:

UCB Biopharma, Development Sciences, Braine l'Alleud, Belgium (F.B)

Translational DMPK & Safety, IPSEN Innovation 5 avenue du Canada, ZI Courtaboeuf, Les Ulis,France (J.O)

Clinical Pharmacology, Drug Metabolism and Pharmacokinetics, MedImmune, Cambridge, United Kingdom (K.B)

Calvagone, Liergues, France (P.P, E.H)

RUNNING TITLE PAGE:

Running title:

Prediction of human nonlinear PK of a new Bcl-2 inhibitor

Corresponding author:

Pierrillas Philippe

Address:

Faculté de Médecine & Maïeutique Lyon Sud Charles Mérieux

165 chemin du Grand Revoyet – BP 12

69921 Oullins cedex

France

Telephone:

+ (33) 4 26 23 59 25

Fax numbers:

+ (33) 4 26 23 59 76

Email:

philippe.pierrillas@gmail.com

Number of text pages: 37

Number of tables: 4

Number of figures: 3 (+3 supplemental)

Number of references: 50

Number of words in the abstract: 202

Number of words in the introduction: 685

Number of words in the discussion: 792

List of non-standard abbreviations:

PK, Pharmacokinetic; PBPK, Physiologically based pharmacokinetics; RMSE, Root mean square error;AFE, Average fold error; LOQ, Limit of quantification; IV, Intravenous; PO, per os; AUC: area under the curve, BDDCS, Biopharmaceutical drug disposition classicaition system; SCID, Severe Combined Immuno-Deficient; CYP, Cytochrome, LC-MSMS, liquid chromatography coupled with mass spectrometry in tandem; S 55746, (S)-N-(4-hydroxyphenyl)-3-(6-(3-(morpholinomethyl)-

DMD Fast Forward. Published on April 2, 2019 as DOI: 10.1124/dmd.118.085605
This article has not been copyedited and formatted. The final version may differ from this version.

1,2,3,4-tetrahydroisoquinoline-2-carbonyl)benzo[d][1,3]dioxol-5-yl)-N-phenyl-5,6,7,8-tetrahydroindolizine-1-carboxamide

Recommended section assignment: Drug Discovery and Translational Medicine

ABSTRACT

S 55746 ((S)-N-(4-hydroxyphenyl)-3-(6-(3-(morpholinomethyl)-1,2,3,4-tetrahydroisoquinoline-2-carbonyl)benzo[d][1,3]dioxol-5-yl)-N-phenyl-5,6,7,8-tetrahydroindolizine-1-carboxamide) is a new selective Bcl-2 inhibitor developed by Servier Laboratories and used to restore apoptosis functions in cancer patients. The aim of this work was to develop a translational approach using physiologically based (PB) pharmacokinetic (PK) modeling for interspecies extrapolation to anticipate the nonlinear PK behavior of this new compound in patients. A PBPK mouse model was first built using a hybrid approach, defining scaling factors (determined from in vitro data) to correct *in vitro* clearance parameters and predicted Kp values. The qualification of the hybrid model using these empirically determined scaling factors was satisfactorily completed with rat and dog data, allowing extrapolation of the PBPK model to humans. Human PBPK simulations were then compared to clinical trial data from a phase 1 trial in which the drug was given orally and daily to cancer patients. Human PBPK predictions were within the 95% prediction interval for the 8 dose levels, taking into account both the nonlinear dose and time dependencies occurring in S 55746 kinetics. Thus, the proposed PK interspecies extrapolation strategy, based on preclinical and *in vitro* information and physiological assumptions, could be a useful tool for predicting human plasma concentrations at the early stage of drug development.

DMD Fast Forward. Published on April 2, 2019 as DOI: 10.1124/dmd.118.085605
This article has not been copyedited and formatted. The final version may differ from this version.

Introduction

The development of a new chemical entity is a long and expensive process. According to several studies (Kola and Landis, 2004), the rate of approval in the field of oncology after entry into phase 1 is approximately 5%, among the lowest of all therapeutic areas. At the beginning of the 1990s, the main reasons for the high attrition rate were a lack of efficacy and unfavorable pharmacokinetics (PK). For this reason, improvement of drug selection at the earliest stage of development based on PK properties (absorption, distribution, metabolism, and excretion) has been encouraged, and the extrapolation of preclinical data to human has been performed much earlier in the development process.

In this way, preclinical information can be a precious resource for predicting the behavior of a compound in humans and therefore can be decisive for "go/no go" decisions. Several methods with different degrees of complexity have been described to predict human PK from non-clinical settings. The most empirical approach for interspecies PK extrapolation is based on the prediction of human PK parameters (clearance, volume of distribution) by allometric scaling (Boxenbaum, 1982; Mordenti, 1986; West et al., 2002; Tang and Mayersohn, 2006) and has been widely used in recent decades. Other more sophisticated strategies have also been developed (Dedrick, 1973; Wajima et al., 2004), based on the assumption that concentration–time profiles of a drug from a variety of species could be superimposed when the curve axes were normalized (by mean residence time, body weight, or dose per kilogram). However, those techniques can be applied only to drugs with linear kinetics and thus have a limited range of applications.

With the progress of *in vitro* experiments and the availability of microsomes and hepatocytes from different species, human clearance parameters could be better determined thanks to the development of *in vitro*/*in vivo* extrapolation (Houston and Carlile, 1997; Houston, 2013). The use of PBPK (physiologically based pharmacokinetic) modeling

(Rostami-Hodjegan et al., 2012) can be an attractive strategy for predicting drug PK thanks to the differentiation of system-specific parameters from drug-specific parameters. Unlike empirical and classical compartmental models, which can be useful to describe data, PBPK models use physiological concepts that facilitate interspecies extrapolation. In a PBPK model, compartments represent tissues or organs; their volumes are set to the real physical volumes, and the different organ-specific blood flows are also considered. In this approach, the disposition profiles are predicted from the physico-chemical properties of the compound and the species-specific physiological parameters (Espie et al., 2009; Jones and Rowland-Yeo, 2013).

Most interspecies extrapolation studies deal with compounds presenting linear PK processes, and few studies have tried to scale the kinetics of drugs exhibiting nonlinear behavior (Dong et al., 2011; Chen et al., 2013) from preclinical studies to clinical trials. In those studies, a Michaelis–Menten equation (Michaelis et al., 2011) has been used to describe the nonlinear phenomenon, and correlations have been calculated using a power law model (Dedrick, 1973) (according to body weight) for the V_m and K_m parameters to predict human parameters. Even if acceptable predictions have been made at some doses, though, difficulties have still been highlighted regarding the ability to capture both linear and nonlinear processes simultaneously (Dong et al., 2011; Chen et al., 2013).

This study focused on the compound S 55746 ((S)-N-(4-hydroxyphenyl) -3- (6-(3-(morpholinomethyl) - 1,2,3,4-tetrahydroisoquinoline -2- carbonyl)benzo [d] [1,3]dioxol-5-yl)-N-phenyl -5,6,7,8-tetrahydroindolizine -1- carboxamide), which was identified as a new Bcl-2 inhibitor. Bcl-2 family proteins largely mediate the mitochondrial apoptotic pathway (Bagci et al., 2006), and in many cancers, apoptosis is affected by Bcl-2 anti-apoptotic protein overexpression (Cosulich et al., 1997; Ottilie et al., 1997), impairing the cell's ability to undergo normal apoptosis (Reed, 2004). Therefore, by inhibiting the Bcl-2 protein, S

55746 can reactivate apoptosis and decrease tumor growth. S 55746 has shown a nonlinear PK during preclinical studies, which presents challenges for interspecies scaling of its PK. The aim of this work therefore was (i) to propose a PK extrapolation strategy based on PBPK modeling, (ii) to predict its PK behavior in humans based on preclinical studies, and (iii) to compare our predictions to the data from the first-in-human trial of S 55746.

DMD Fast Forward. Published on April 2, 2019 as DOI: 10.1124/dmd.118.085605
This article has not been copyedited and formatted. The final version may differ from this version.

Material and Methods

In Vitro Methods

Protein Binding. S 55746 (Figure 1) was provided by Servier Laboratories. The unbound fraction in plasma ($f_{u,p}$) of [14C]-S 55746 was determined in animals and humans by dialysis using the Rapid Equilibrium Dialysis device system (Thermo-Fischer, Massachusetts) at the concentrations of 500, 5000 and 50000 ng/mL for all species. Aliquots of spiked plasma were placed into the sample chamber, and samples of non-spiked dialysis buffer were added to the buffer chamber. The plates were covered and incubated at 37°C at 500 rpm on an orbital shaker (for 1, 3, 4 and 5h). All incubations were performed in triplicate and analyzed by liquid scintillation counting.

Blood to Plasma Partition. The blood to plasma concentration ratio ($R_{bl:p}$) was determined in triplicate per concentration for all species. Prior to spiking blood, a small aliquot of blood was taken for the determination of the hematocrit. Spiked blood samples were incubated on a roller mixer for 1 h at 37°C and then centrifuged at room temperature. Finally, plasma was transferred into appropriate tubes to be analyzed by liquid scintillation counting to allow the determination of drug concentration. The blood-to-plasma concentration ratio was calculated using the following equation:

$$R_{bl:p} = \frac{C_{bl}}{C_p} \qquad Eq\ 1$$

where C_{bl} and C_p are respectively the drug concentration in blood and plasma.

Microsome and Hepatocyte Clearance Determination.

Microsomal incubations were carried out for different times (0, 7, 17, 30 and 60 min) at 37 °C with human liver microsomes (HLM) with S 55746 at a final concentration of 0.1 and 40 µM. Reactions were initiated by addition of nicotinamide adenine dinucleotide phosphate (NADPH) after a 10 minutes pre-incubation time. During incubation, aliquots were sampled

at each incubation time and the enzymatic reaction was stopped by protein precipitation using methanol.

For hepatocytes, S 55746 was incubated for different time points (0, 5, 10, 20, 30, 60 and 100 min) in William EC medium (Thermo-Fischer, Massachusetts). Reactions were initiated by the addition of S 55746. During incubation, aliquots were sampled at each incubation time and the enzymatic reaction was stopped by protein precipitation using acetonitrile.

Samples were then centrifuged and the supernatants transferred to analysis plates, followed by analysis using liquid chromatography coupled with mass spectrometry in tandem (LC-MS/MS).

The K_m and V_m parameters of S 55746 in HLM and in hepatocytes were determined via substrate disappearance kinetics. Since the enzyme activity decreases with time, V_m can be described by:

$$V_m = V_{m0} \cdot e^{-k_d \cdot t} \qquad Eq\ 2$$

where V_{m0} is the initial V_m and k_d the inactivation constant for the degradation of enzyme activity.

The model used to describe the disappearance of the substrate was therefore:

$$\frac{dS}{dt} = -\frac{V_m \cdot [S]}{K_m + [S]} \qquad Eq\ 3$$

The data were analysed with the nonlinear analysis software WinNonlin Version 5.1 (Pharsight Corporation, USA). The K_m and V_m parameters were estimated with inclusion of microsomal binding data.

The determination of the intrinsic clearance was calculated using the following formulas according to microsome or hepatocyte experiments:

$$CL_{int,vitro,mic/hep} = \frac{V_m}{K_m + C_u} \qquad Eq\ 4$$

$$CL_{int,vivo} = CL_{int,vitro,mic} \cdot MPPGL \cdot Liver\ Weight \qquad Eq\ 5$$

DMD Fast Forward. Published on April 2, 2019 as DOI: 10.1124/dmd.118.085605
This article has not been copyedited and formatted. The final version may differ from this version.

where $CL_{int,vivo}$ is the intrinsic clearance for the whole organ, $CL_{int,vitro,mic}$ is the intrinsic clearance determined with the microsomal system, and MPPGL represents the microsomal protein per gram of liver of the relevant species; and

$$CL_{int,vivo} = CL_{int,vitro,hep} \cdot HPGL \cdot Liver\ Weight \qquad Eq\ 6$$

where $CL_{int,vitro,hep}$ is the intrinsic clearance measured by the hepatocyte system and HPGL represents the number of hepatocytes per gram of liver.

Identification of Enzymes Involved in Human Hepatic Metabolism. Cytochrome (CYP) contribution was determined *via* clearance experiments with S 55746 and recombinant human CYPs (*rh*CYPs) 1A2, 2C8, 2C9, 2C19, 2D6, and 3A4. S 55746 was incubated with each individual *rh*CYP for 0 min, 7 min, 17 min, 30 min, or 60 min.

The relative contribution of each CYP enzyme to the oxidative part of the microsomal clearance of S 55746 was estimated by comparing each individual CYP's intrinsic clearance ($CL_{int,rhCYP}$) to the sum of individual CYP intrinsic clearance ($\sum CL_{int,rhCYP}$).

$$fm(\%) = \frac{CL_{int},rhCYP}{\sum CL_{int},rhCYP} \qquad Eq\ 7$$

A relative activity factor (RAF) was estimated from the ratio of the intrinsic clearance (values for CYP specific probe substrates using rhCYP and using human liver microsomes using the following equation:

$$RAF = \frac{CL_{int},rhCYP}{CL_{int},HLM} \qquad Eq\ 8$$

The concentration of bactosomes to be used in the incubation was calculated from the concentration of HLM used as standard for intrinsic clearance measurement, using the following equation:

$$[rhCYP] = \frac{[HLM]}{RAF} \qquad Eq\ 9$$

Where [rhCYP] is the bactosomal protein concentration and [HLM] is the microsomal protein concentration.

DMD Fast Forward. Published on April 2, 2019 as DOI: 10.1124/dmd.118.085605
This article has not been copyedited and formatted. The final version may differ from this version.

Supernatants were analyzed using a turboflow LC-MS/MS Platinum Mass Spectrometer to assay S 55746 concentrations. Orthogonal assays using microsomes and CYP inhibitors were conducted in order to confirm the results.

Assessment of Mechanism-based Inhibition in Humans liver microsomes. The possible existence of mechanism-based inhibition (Obach et al., 2007) of CYP3A4 was also investigated. Human liver microsomes were pre-warmed with S 55746 (0, 0.25, 0.5, 1, 2, 3, 10 and 30 μM) for 5 min at 37°C. The pre-incubation was initiated by addition of NADPH or buffer, and at different pre-incubation times (0, 2, 4, 6, 8, 12 and 14 minutes), an aliquot of the pre-incubate was collected and added to a vial containing midazolam (Sekiguchi et al., 2011). After an incubation of 7 min, reactions were terminated by addition of methanol. Samples were placed on ice before centrifugation. Supernatants were analyzed using LC-MS/MS for measurement of hydroxymidazolam concentration. Calculations and regression analysis were performed using Excel™ 2003 (Microsoft Corporation, Roselle, USA) and Xlfit4 (IDBS software, Guildford, UK).

A value for k_{inact} (maximum inactivation rate constant) and K_{app} (concentration which produces the half maximal rate of inactivation) was determined by nonlinear regression analysis. The data were fitted to the following equation:

$$k_{obs} = \frac{k_{inact} \cdot [I]}{K_{app} + [I]} \qquad Eq\ 10$$

where k_{obs} is the slope observed when representing the natural logarithm of percent remaining activity against the pre-incubation time, k_{inact} is the maximum inactivation rate constant, [I] is the inhibitor concentration and K_{app} is the concentration which produces the half maximal rate of inactivation.

Induction.

Isolated human hepatocytes cultured on type I collagen plates were used to assess the induction potential of S 55746. For 3 days, these human hepatocytes were treated with S

55746 at 0.1, 1, 2.5, 5, or 10 µM omeprazole (a known inducer of human CYP1A), phenobarbital (a known inducer of human CYP2B6), or rifampicin (a known inducer of human CYP3A). After 3 days, the hepatocytes were incubated with the cytochrome P450 substrates phenacetin (CYP1A2), bupropion (CYP2B6), and midazolam (CYP3A4) for assessment of enzyme activity.

Following the incubation, hepatocytes were harvested to isolate RNA (ribonucleic acid), analyzed by quantitative reverse transcriptase polymerase chain reaction. The obtained activities were compared to those of control cultures not exposed to the test compounds or to the reference CYP inducers. The results were expressed as fold induction compared to the control conditions or as a percentage of the reference inducer CYP activity or mRNA expression increase. When a concentration-dependent increase of CYP mRNA was observed and a maximum fold change was reached during the experiments, the data (fold induction) were processed for the determination of induction parameters (Indmax, maximal fold induction and Ind C50, concentration at which there is a 50% maximal induction effect) by non-linear regression fitting of the data.

Apparent Permeability: P_{app} Determination. The Caco-2 cell line (Hilgers et al., 1990) was cultured in Dulbecco's modified Eagle's Medium containing 10% (v/v) of fetal calf serum, 1% L-glutamine, nonessential amino acids, antibiotics, and amphotericin. Cells were seeded at 90,000 cells per cm^2 onto a microporous membrane of 24-multiwell insert plates so that apical (A) and basolateral (B) media would be separated by the cell monolayer. Cells were maintained at 37°C in an atmosphere of 95% air and 5% CO_2 and used between 21 and 30 days post seeding. S 55746 was incubated at 10 µM in the apical chamber. Samples (duplicate) were collected at 30 and 90 min in the basolateral chamber and analyzed

DMD Fast Forward. Published on April 2, 2019 as DOI: 10.1124/dmd.118.085605
This article has not been copyedited and formatted. The final version may differ from this version.

by LC-MSMS. Reference compounds $P_{app\ A\text{-}B}$ (cimetidine, propranolol) were used to determine the calibration curve of the Caco-2 model.

Table 1 shows the *in vitro* and *in silico* parameters for all species.

PBPK Modeling

The PBPK modeling strategy was based on the use of either *in vitro* or *in vivo* data (according to a retrograde approach) depending on the quality of the predictions (Peters, 2008). Simcyp software, version 14 (Jamei et al., 2009a; Jamei et al., 2013), was used to perform PBPK modeling.

Distribution. In the full PBPK distribution model, we assumed that the drug distributes instantaneously and homogeneously within each tissue and that its uptake in each tissue is limited by the blood flow (perfusion limited). The rate of change of the drug in a non-eliminating tissue is described by the following differential equation (Nestorov, 2003; Jones et al., 2009):

$$V_T \cdot \frac{dC_T}{dt} = Q_T \cdot \left(C_{a,bl} - C_{v,bl,T}\right) = Q_T \cdot \left(C_{a,bl} - \frac{C_T}{Kp_{T:bl}}\right) \qquad Eq\ 11$$

where Q_T is the tissue blood flow and V_T is the volume of the tissue. The subscript *T* denotes the tissue, the subscript *a* represents the artery, *bl* denotes the blood, and *v* the vein. $C_{a,bl}$ and $C_{v,bl,T}$ refer to the concentration in the arterial blood entering the tissue and the concentration in the venous blood leaving the tissue, respectively, and $Kp_{T:bl}$ is the coefficient partition between the tissue and the blood.

It has been considered that the drug might be eliminated only from liver where the rate of change of the drug can be expressed by:

$$V_h \cdot \frac{dC_h}{dt} = Q_h \cdot \left(C_{a,bl} - C_{v,bl,h}\right) - CL_{int,vivo} \cdot C_{u,h} \qquad Eq\ 12$$

where the subscript *h* denotes the liver, $CL_{int,vivo}$ the intrinsic *in vivo* clearance, and $C_{u,h}$ the unbound concentration in the liver.

DMD Fast Forward. Published on April 2, 2019 as DOI: 10.1124/dmd.118.085605
This article has not been copyedited and formatted. The final version may differ from this version.

The equations of Poulin and Theil (Poulin and Theil, 2002a; Poulin and Theil, 2002b), modified by Berezhkovskiy (Berezhkovskiy, 2004), and the equations of Rodgers and Rowland (Rodgers et al., 2005a; Rodgers et al., 2005b; Rodgers and Rowland, 2006; Rodgers and Rowland, 2007) were compared to predict tissue/plasma partition coefficients ($Kp_{T:p}$) from physico-chemical parameters and the resulting volume of distribution in plasma:

$$V_{SS} = V_{bl} \cdot R_{bl:p} + \sum V_T \cdot Kp_{T:p} \qquad Eq\ 13$$

Clearance. The well-stirred model (Rowland et al., 1973; Pang and Rowland, 1977) was used to determine hepatic clearance $CL_{h,bl}$ from the intrinsic clearance CL_{int}, the hepatic blood flow Q_h, and the unbound fraction in blood $f_{u,bl}$:

$$CL_{h,bl} = \frac{Q_h \cdot f_{u,bl} \cdot CL_{int,vivo}}{Q_h + f_{u,bl} \cdot CL_{int,vivo}} \qquad Eq\ 14$$

Where $f_{u,bl}$ was calculated by dividing the unbound fraction in plasma ($f_{u,p}$) by the blood to plasma ratio.

Oral Absorption. The oral absorption in humans was predicted using the ADAM (Advanced Dissolution, Absorption, and Metabolism) model (Jamei et al., 2009b; Patel et al., 2014) implemented in Simcyp. The ADAM model is a multi-compartmental gastrointestinal (GI) transit model. The GI tract is treated as a one-stomach, seven-small-intestine, and one-colon compartment, and the drug can exist in several states simultaneously: unreleased, undissolved, dissolved, or degraded. In this model, data from apparent permeability experiment (P_{app}) are used to predict the effective permeability across the enterocyte (Sun et al., 2002) and the integration of the dissolution profile of the formulation can be used to determine the fraction of the pharmaceutical active compound released from the formulation over time.

Strategy for Interspecies Qualification. Before performing PBPK simulations in humans, a qualification exercise was performed on different preclinical species. For this qualification with rat and dog PBPK models, the mouse physiological model parameters were

replaced with the corresponding values for rat and dog, and the drug-specific parameters measured in mouse-specific in vitro systems (e.g. CLint, $f_{u,p}$) were replaced with the corresponding values measured in rat and dog in vitro systems. Simulations were carried out based on the dose and administration schedule in the in vivo studies, and the rat and dog PBPK model predictions were evaluated for their goodness of prediction based on the model evaluation criteria described below (see Prediction performances and parameter analyses). Intravenous PK data from two preclinical species, rat and dog, were available to qualify the PBPK approach and to validate interspecies extrapolation.

In Vivo Preclinical PK Studies

All of the animal experiments were reviewed and approved by the ethical committee, and were in general accordance with the animal health and welfare guidelines; it was also ensured there were no other alternative methods than live animals to achieve the study objectives. Severe combined immunodeficient (SCID) female mice, male Wistar rats, and male beagle dogs from Charles River Laboratories were used for PK studies. The oral formulations were different in each species, so only intravenous (IV) studies were considered in preclinical species (mouse, rat, dog) to better characterize clearance and distribution processes.

Mouse Studies. SCID mice (female) were treated with S 55746 by IV bolus of 1, 3, 10, or 25 mg/kg. Blood samples (from the tail or saphenous vein) between 0.083 to 30 h after dose were collected in 2 to 5 mice per time point.

Rat Studies. PK studies in Wistar rat (male) were conducted after an IV infusion administered at the following doses: 0.5, 1.5, or 5 mg/kg. Blood samples (from the tail vein) were collected from 0.17 to 24 h after administration. Three animals were used for each dose level.

Dog Studies. In PK studies in Beagle dog (male), S 55746 was given after a single IV bolus administration. Doses of 0.2 and 1.5 mg/kg were administered to dogs. S 55746 was quantified from 0.17 to 24 h after administration. Data from three dogs were available for each dose.

Clinical Study

Clinical protocols were approved by the French regulatory agency (Agence Nationale de Sécurité du Médicament, or ANSM), and all subjects gave written informed consent for participation in the clinical trials. Dose escalation in the phase I clinical trial was driven by the Continual Reassessment Method (Garrett-Mayer, 2006).

S 55746 was given orally once a day to fasted cancer patients (non-Hodgkin lymphoma, chronic lymphocytic leukemia, and acute myeloid leukemia) for a period of 21 days at different doses (100 mg, 200 mg, 300 mg, 400 mg, 500 mg, 700 mg, 900 mg and 1100 mg). Blood samples were collected over 24 h on the first and eighth days of administration.

Bioanalytical method

The drug concentrations in plasma were determined using liquid chromatography coupled with mass spectrometry in tandem (LC-MS/MS). For this bioanalytical method, samples were thawed at room temperature, vortex mixed and centrifuged. Aliquots of samples were added to the Ostro^{TM} (Waters, Milford, Massachusetts, USA) sample preparation plate with the internal standard (N-(4-{2-[(3aS,9bR)-8-Cyano-1,2,3,3a,4,9b-hexahydrochromeno [3,4-c]pyrrol-2-yl]ethyl}phenyl)acetamide, hydrochloride) to remove proteins and phospholipids. Plates were mixed at room temperature. After elution in 96 well plate, 100 µl of the eluate was mixed and injected directly into the LC-MS/MS system. Analytes were separated using a pentafluorophenyl column (100x2.1 mm, 2.6 µm). Multiple-reaction monitoring was selected

DMD Fast Forward. Published on April 2, 2019 as DOI: 10.1124/dmd.118.085605
This article has not been copyedited and formatted. The final version may differ from this version.

for detection at m/z 711.4 > 624.4. The lower limit of quantification was 1 ng.ml^{-1} for mice studies, and 5 ng.ml^{-1} for rats and dogs studies. For clinical study, the lower limit of quantification was 10 ng.ml^{-1}.

Prediction Performances and Parameter Analyses

Since observed PK data were drug concentrations in plasma, PBPK model-predicted plasma concentrations were obtained by dividing predicted blood concentrations by the blood to plasma ratio.

Non-compartmental Analysis. For *in vivo* studies, the S 55746 plasma concentration–time profiles were analyzed by non-compartmental analysis, and the area under the curve (AUC) was calculated using the log–linear trapezoidal rule.

Assessment of Prediction Accuracy. The accuracy of PBPK prediction was evaluated on AUC and plasma concentrations. The goodness of prediction in each preclinical species was evaluated based on the average fold error (AFE) and on the root mean square error (RMSE) (Sheiner and Beal, 1981). The fold error, AFE, and RMSE were calculated as follows:

$$fold\ error = \frac{PRED}{OBS} \qquad Eq\ 15$$

$$AFE = 10^{\frac{\sum log\ fold\ error}{n}} \qquad Eq\ 16$$

$$RMSE = \sqrt{\frac{\sum(log\ PRED - log\ OBS)^2}{n}} \qquad Eq\ 17$$

where PRED is the prediction, OBS is the observation, and n is the number of samples.

To account for the interindividual variability existing in clinical data, prediction performances were assessed using the 95th confidence interval of the simulated AUC and maximal concentration, C_{max} (Abduljalil et al., 2014).

Results

S 55746 compound

From in vitro experiments (data shown in Table 1), S 55746 was shown to be an ampholyte compound with a high lipophilicity. In all species tested, S 55746 was found to be highly bound to plasma proteins and extensively metabolized (mainly by CYP450 enzymes). Also, S 55746 exhibits both enzymatic induction properties and mechanism based inhibition on CYP3A4.

PBPK Modeling in Mice

A basic PBPK approach was first applied in mice using the intrinsic clearance parameters determined with *in vitro* experiments (and extrapolated to *in vivo* using physiological scaling factors) and distribution parameters predicted from physico-chemical properties. This approach resulted in poor prediction accuracy and did not account for the nonlinear elimination process seen *in vivo* (data not shown).

A comparison with a hybrid PBPK approach (Sayama et al., 2012; Sayama et al., 2013) was undertaken next. In this case, the *in vivo* clearance and *in vivo* volume of distribution determined with a previous compartmental model analysis (Pierrillas et al., 2018) were used to calculate empirical scaling factors (SFs) in the PBPK model. Parameters determined from the compartmental analysis are shown in Table 2.

In addition, the Poulin and Theil method corrected by Berezhkovskiy provided better performances for the $Kp_{T:p}$ calculation than the Rodgers and Rowland method (the Rodgers and Rowland method implemented in Simcyp software better predicts the volume of distribution for strong bases whereas S 55746 is an ampholyte compound).

Regarding elimination, the nonlinear elimination uncovered in the previous compartmental analysis (Pierrillas et al., 2018) was incorporated into the PBPK model: a

DMD Fast Forward. Published on April 2, 2019 as DOI: 10.1124/dmd.118.085605
This article has not been copyedited and formatted. The final version may differ from this version.

back calculation of the *in vivo* clearance parameters was done to insert these parameters into the PBPK model according to the following relationships (demonstration in the appendix):

$$\begin{cases} V_m = V_{m,int} & \textit{Eq 18} \\ K_m = \frac{K_{m,int}}{f_{u,bl}} + \frac{V_{m,int}}{Q_h} & \textit{Eq 19} \end{cases}$$

Where V_m is the in vivo maximum rate of elimination, $V_{m,int}$ is the intrinsic maximum rate of elimination, K_m is the drug concentration in plasma corresponding to 50% of the maximum rate of elimination, $K_{m,int}$ is the intrinsic drug concentration corresponding to 50% of the intrinsic maximum rate of elimination, $f_{u,bl}$ the unbound fraction in blood, and Q_h the hepatic blood flow.

In addition, the considered compound was demonstrated to have a low hepatic extraction coefficient (E_H < 0.3) during PK studies in mice. Consequently, the *in vivo* clearance could be approximated by the intrinsic clearance times the unbound fraction:

$$\begin{cases} V_m = V_{m,int} & \textit{Eq 20} \\ K_m = \frac{K_{m,int}}{f_{u,bl}} & \textit{Eq 21} \end{cases}$$

A predictions versus observations plot of plasma concentrations performed with the hybrid approach is shown in Figure 2, and all measures of predictive performances are reported in Table 3. PBPK predictions resulting from the hybrid approach and the descriptions of concentration–time profiles (shown in the supplemental material) were more satisfactory than those obtained with the classical method (using in vitro CL_{int}). The ratios $\frac{AUC_{Obs}}{AUC_{Pred}}$ for each dose are in the range of acceptance (0.5- to 2-fold). In the observed dose range in mice, AFE ranged from 0.672 to 1.42 and RMSE varied from 0.138 to 0.491. These performances are acceptable because no interindividual variability has been taken into

DMD Fast Forward. Published on April 2, 2019 as DOI: 10.1124/dmd.118.085605
This article has not been copyedited and formatted. The final version may differ from this version.

account in the proposed PBPK model. The hybrid approach was therefore selected for use in the interspecies extrapolation, and the subsequent qualification with rat and dog.

Qualification of the PBPK Approach with Rat and Dog Data

As the hybrid approach was satisfactory in mice, SFs for clearance and distribution parameters were calculated from the mouse as follows:

$$SF_{V_m} = \frac{V_{m_{vitro}}}{V_m} \qquad Eq\ 22$$

$$SF_{K_m} = \frac{K_{m_{vitro}}}{K_m} \qquad Eq\ 23$$

$$SF_{Kp} = \frac{V_{ss,vivo} - V_{bl} \cdot R_{bl:p}}{\sum V_T \cdot Kp_{T:p}} \qquad Eq\ 24$$

Where SF_{Km}, SF_{Vm} and SF_{Kp} are respectively the scaling factors for K_m, V_m and the coefficient of patition Kp, $K_{m\ vitro}$, $V_{m\ vitro}$ are the clearance parameters determined from in vitro experiment and K_m , V_m are the in vivo clearance and distribution parameters determined from the previous compartmental analysis (Pierrillas et al., 2018).

To qualify the hybrid PBPK approach, clearance and distribution parameters were predicted in rat and dog using SF defined in mice, assuming that the discrepancies between *in vitro* and *in vivo* parameters in other species had a similar origin to that in mice. For both species, predictions versus observations plots are presented in Figure 2, concentration–time profiles for all of the qualification exercises are presented in the supplemental material (Supplemental Figure 1), and predictive performances are shown in Table 4.

For rat data, concentration–time profiles were well predicted; furthermore, the $\frac{AUC_{Obs}}{AUC_{Pred}}$ ratios were acceptable ($\frac{AUC_{Obs}}{AUC_{Pred}}$ ratios between 1.10 and 1.20). Concerning dog data, the exposure parameters were also satisfactory ($\frac{AUC_{Obs}}{AUC_{Pred}}$ ratios less than 2 and above 0.5), but the

concentration–time profiles were less well described (especially the terminal phase) than in rat.

Regarding prediction performances of plasma concentrations, AFE values for both species were not out of the limits of [0.5, 2], and RMSE did not exceed 27.6%. These results implied that the predictions were acceptable.

Thus, the qualification of the hybrid approach with the application of the SFs was considered satisfactory with rat and dog data. For this reason, the same strategy was selected for the prediction of human PK.

PBPK Predictions Challenged with Clinical Data

The SFs defined in mice were applied to human in vitro clearance and distribution parameters. In addition, the metabolic pathway of S 55746 determined from *in vitro* studies on human cells was incorporated into the model. *In vitro* studies highlighted that CYPs were responsible for 85% of the metabolism of S 55746 and furthermore that CYP3A4 was the main isoenzyme involved (97% of CYP-mediated metabolism) (Table 1). Accordingly, liver clearance was described as the sum of CYP3A4-dependent clearance (82.5%) and CYP3A4-independent clearance (17.5%). Because this CYP3A4-independent clearance likely resulted from uridine 5'-diphospho-glucuronosyltransferase (UGT enzymes), an interindividual variability of 75% was added to this parameter (Court, 2010). Concerning the absorption process, the dissolution profile of the drug in formulation and the *in vitro* permeability data from Caco-2 experiments were added to the human PBPK model. The predictions were better using hepatocyte data rather than microsomal data (data not shown), which is certainly due to the involvement of drug conjugation.

For both PK sampling days (day 1 and day 8), the predicted concentration-time profiles were in good agreement with the observed data (Supplemental Figure 2). Furthermore,

despite the large interindividual variability, our approach satisfactorily predicted the observed AUC and C_{max} values for patients at all doses (Figure 3), permitting the qualification of the PBPK extrapolation strategy at eight dose levels. Exploring the PK characteristics of S 55746 in humans by simulation of the PBPK model at the different doses (Supplemental Figure 3), S 55746 PK appeared to be proportional to the dose in the studied dose range.

DMD Fast Forward. Published on April 2, 2019 as DOI: 10.1124/dmd.118.085605
This article has not been copyedited and formatted. The final version may differ from this version.

Discussion

A new approach has been developed for predicting the nonlinear PK characteristics in humans of a new Bcl-2 inhibitor using PBPK modeling and interspecies extrapolation. The application of the classical interspecies prediction methods (allometry, Dedrick method, Wajima method) was not appropriate because of the violation of their main assumptions (nonlinear PK of S 55746 in nonclinical species). Consequently, *in vivo* mouse data were used to build a hybrid PBPK model, and SFs were derived to correct *in vitro* clearance (V_m, K_m) and distribution (Kp) parameters. Since SFs determined in mice were applied to other species, this implied that the reasons for divergence between in vitro and in vivo parameters were similar among species.

The use of *in vitro* parameters with physiological scaling factors directly as input into the PBPK model in mice led to poor prediction accuracy and particularly did not reflect the nonlinear behavior of the compound seen during *in vivo* preclinical studies along with other factors not taken into account in the commonly used (or physiological) extrapolation factors. This was accounted for by the development of a hybrid approach defining SFs in the mouse for both V_m and K_m parameters, and was qualified using two other non-clinical species (rat and dog).

The high value of RMSE found in the model evaluation exercise in mice is probably due to the fact that the Simcyp animal module (version 13) does not incorporate physiological interindividual variability. In consequence, all of the variability highlighted during the previous compartmental population analysis of *in vivo* mouse data (Pierrillas et al., 2018) was considered as residual variability in the PBPK analysis and consequently inflated RMSE values.

The use of SFs has always been controversial regarding the rationale and foundations. The need for additional SFs between *in vitro* and *in vivo* values for clearance and distribution

parameters can arise from many processes. In this example, a likely explanation could be the implication of transporters for distribution and elimination of the compound. Indeed, during clearance determination on microsome or hepatocyte suspension, transporters are not functional, and consequently, the measurement does not represent the whole of what is occurring *in vivo*. S 55746 is a BDDCS (Biopharmaceutics Drug Disposition Classification System) class 2 compound (Benet et al., 2011; Broccatelli et al., 2012), so this assumption is reinforced. In addition, approximately 50% of S 55746 molecules are positively ionized at physiological pH, confirming the plausibility of the involvement of cation transporters, such as organic cation transporters (Koepsell et al., 2007; Giacomini et al., 2010).

The implication of transporters affecting the distribution process can also be invoked to explain the need for SFs for Kp values. Other arguments in favor of SF could be an incorrect assessment of the plasma protein binding ($f_{u,p}$) or a non-consideration of a tissue-binding component in the Kp calculation.

Furthermore, the interspecies extrapolation with the hybrid approach was based on the assumption that the reasons for divergence between *in vitro* and *in vivo* parameters were similar across species. This can be considered as a strong hypothesis but was supported by the data; however, finding mechanistic explanations for SF remains a challenge for future research.

Regarding the human data, the best results were obtained using the clearance (in combination with the SFs) determined from hepatocytes rather than microsomes. The possible involvement of conjugation or glucuronidation (which is not assessed with microsome experiments) can explain this result.

In addition, *in vitro* studies revealed that S 55746 affected its own metabolism (CYP3A4) by mechanism-based inhibition and induction. The predicted combination of both phenomena seems to reflect the observed kinetic profile of S 55746. However, the power to

DMD Fast Forward. Published on April 2, 2019 as DOI: 10.1124/dmd.118.085605
This article has not been copyedited and formatted. The final version may differ from this version.

detect an invalidation of the model is low because of the small population size combined with the large observed variability.

On the other hand, for few patients (over all doses), the PBPK model does not seem to capture C_{max} and exposure parameters very well. Nevertheless, investigation showed that these patients were also given proton-pump inhibitors; these medicines increase the pH in the stomach, leading to lower solubility of S 55746 and consequently to a reduction in drug absorption.

Overall, the combination of this PBPK model-building approach with interspecies extrapolation led to acceptable and satisfactory predictions in humans at different doses and described well all of the kinetic processes observed so far. Furthermore, the PBPK model-building strategy could have important applications in the development of drugs with nonlinear kinetics by helping to anticipate PK behavior using all information available from preclinical and *in vitro* studies at the earliest stage. In addition, the combination of this PBPK model with a pharmacodynamic model could be useful for early forecasting of efficacy in humans, to propose doses for testing in clinical studies, to optimize the design of phase 1 studies, and ultimately for making "go/no go" decisions.

Acknowledgments

Authorship Contributions

Participated in research design: Pierrillas P.B, Hénin E., Ogier J., Amiel M., Kraus-Berthier L., Bouzom F.,Tod M.

Conducted experiments: Kraus-Berthier L.

Contributed new reagents or analytic tools:

Performed data analysis: Pierrillas P.B, Hénin E. Tod M.

Wrote or contributed to the writing of the manuscript: Pierrillas P.B, Hénin E., Ball K., Ogier J., Amiel M., Chenel M., Bouzom F., Tod M.

References

Abduljalil K, Cain T, Humphries H, and Rostami-Hodjegan A (2014) Deciding on Success Criteria for Predictability of Pharmacokinetic Parameters from In Vitro Studies: An Analysis Based on In Vivo Observations. *Drug metabolism and disposition: the biological fate of chemicals*.

Bagci EZ, Vodovotz Y, Billiar TR, Ermentrout GB, and Bahar I (2006) Bistability in apoptosis: roles of bax, bcl-2, and mitochondrial permeability transition pores. *Biophys J* **90:**1546-1559.

Benet LZ, Broccatelli F, and Oprea TI (2011) BDDCS applied to over 900 drugs. *The AAPS journal* **13:**519-547.

Berezhkovskiy LM (2004) Determination of volume of distribution at steady state with complete consideration of the kinetics of protein and tissue binding in linear pharmacokinetics. *Journal of pharmaceutical sciences* **93:**364-374.

Boxenbaum H (1982) Interspecies scaling, allometry, physiological time, and the ground plan of pharmacokinetics. *Journal of pharmacokinetics and biopharmaceutics* **10:**201-227.

Broccatelli F, Cruciani G, Benet LZ, and Oprea TI (2012) BDDCS class prediction for new molecular entities. *Mol Pharm* **9:**570-580.

Chen T, Mager DE, and Kagan L (2013) Interspecies modeling and prediction of human exenatide pharmacokinetics. *Pharmaceutical research* **30:**751-760.

Cosulich SC, Worrall V, Hedge PJ, Green S, and Clarke PR (1997) Regulation of apoptosis by BH3 domains in a cell-free system. *Curr Biol* **7:**913-920.

Court MH (2010) Interindividual variability in hepatic drug glucuronidation: studies into the role of age, sex, enzyme inducers, and genetic polymorphism using the human liver bank as a model system. *Drug metabolism reviews* **42:**209-224.

Dedrick RL (1973) Animal scale-up. *Journal of pharmacokinetics and biopharmaceutics* **1:**435-461.

Dong JQ, Salinger DH, Endres CJ, Gibbs JP, Hsu CP, Stouch BJ, Hurh E, and Gibbs MA (2011) Quantitative prediction of human pharmacokinetics for monoclonal antibodies: retrospective analysis of monkey as a single species for first-in-human prediction. *Clinical pharmacokinetics* **50:**131-142.

Espie P, Tytgat D, Sargentini-Maier ML, Poggesi I, and Watelet JB (2009) Physiologically based pharmacokinetics (PBPK). *Drug metabolism reviews* **41:**391-407.

Garrett-Mayer E (2006) The continual reassessment method for dose-finding studies: a tutorial. *Clin Trials* **3:**57-71.

Giacomini KM, Huang SM, Tweedie DJ, Benet LZ, Brouwer KL, Chu X, Dahlin A, Evers R, Fischer V, Hillgren KM, Hoffmaster KA, Ishikawa T, Keppler D, Kim RB, Lee CA, Niemi M, Polli JW, Sugiyama Y, Swaan PW, Ware JA, Wright SH, Yee SW, Zamek-Gliszczynski MJ, and Zhang L (2010) Membrane transporters in drug development. *Nat Rev Drug Discov* **9:**215-236.

Hilgers AR, Conradi RA, and Burton PS (1990) Caco-2 cell monolayers as a model for drug transport across the intestinal mucosa. *Pharmaceutical research* **7:**902-910.

Houston JB (2013) Prediction of human pharmacokinetics in 2013 and beyond. *Drug metabolism and disposition: the biological fate of chemicals* **41:**1973-1974.

Houston JB and Carlile DJ (1997) Prediction of hepatic clearance from microsomes, hepatocytes, and liver slices. *Drug metabolism reviews* **29:**891-922.

Jamei M, Marciniak S, Edwards D, Wragg K, Feng K, Barnett A, and Rostami-Hodjegan A (2013) The simcyp population based simulator: architecture, implementation, and quality assurance. *In silico pharmacology* **1:**9.

Jamei M, Marciniak S, Feng K, Barnett A, Tucker G, and Rostami-Hodjegan A (2009a) The Simcyp population-based ADME simulator. *Expert opinion on drug metabolism & toxicology* **5:**211-223.

Jamei M, Turner D, Yang J, Neuhoff S, Polak S, Rostami-Hodjegan A, and Tucker G (2009b) Population-based mechanistic prediction of oral drug absorption. *The AAPS journal* **11:**225-237.

Jones H and Rowland-Yeo K (2013) Basic concepts in physiologically based pharmacokinetic modeling in drug discovery and development. *CPT: pharmacometrics & systems pharmacology* **2:**e63.

Jones HM, Gardner IB, and Watson KJ (2009) Modelling and PBPK simulation in drug discovery. *The AAPS journal* **11:**155-166.

Koepsell H, Lips K, and Volk C (2007) Polyspecific organic cation transporters: structure, function, physiological roles, and biopharmaceutical implications. *Pharmaceutical research* **24:**1227-1251.

Kola I and Landis J (2004) Can the pharmaceutical industry reduce attrition rates? *Nat Rev Drug Discov* **3:**711-715.

Michaelis L, Menten ML, Johnson KA, Goody RS, Michaelis L, and Menten ML (2011) The original Michaelis constant: translation of the 1913 Michaelis-Menten paper. *Biochemistry* **50:**8264-8269.

Mordenti J (1986) Man versus beast: pharmacokinetic scaling in mammals. *Journal of pharmaceutical sciences* **75:**1028-1040.

Nestorov I (2003) Whole body pharmacokinetic models. *Clinical pharmacokinetics* **42:**883-908.

Obach RS, Walsky RL, and Venkatakrishnan K (2007) Mechanism-based inactivation of human cytochrome p450 enzymes and the prediction of drug-drug interactions. *Drug metabolism and disposition: the biological fate of chemicals* **35:**246-255.

Ottilie S, Diaz JL, Horne W, Chang J, Wang Y, Wilson G, Chang S, Weeks S, Fritz LC, and Oltersdorf T (1997) Dimerization properties of human BAD. Identification of a BH-3 domain and analysis of its binding to mutant BCL-2 and BCL-XL proteins. *The Journal of biological chemistry* **272:**30866-30872.

Pang KS and Rowland M (1977) Hepatic clearance of drugs. I. Theoretical considerations of a "well-stirred" model and a "parallel tube" model. Influence of hepatic blood flow, plasma and blood cell binding, and the hepatocellular enzymatic activity on hepatic drug clearance. *Journal of pharmacokinetics and biopharmaceutics* **5:**625-653.

Patel N, Polak S, Jamei M, Rostami-Hodjegan A, and Turner DB (2014) Quantitative prediction of formulation-specific food effects and their population variability from in vitro data with the physiologically-based ADAM model: a case study using the BCS/BDDCS Class II drug nifedipine. *European journal of pharmaceutical sciences : official journal of the European Federation for Pharmaceutical Sciences* **57:**240-249.

Peters SA (2008) Evaluation of a generic physiologically based pharmacokinetic model for lineshape analysis. *Clinical pharmacokinetics* **47:**261-275.

Pierrillas PB, Henin E, Ogier J, Kraus-Berthier L, Chenel M, Bouzom F, and Tod M (2018) Tumor Growth Inhibition Modelling Based on Receptor Occupancy and Biomarker Activity of a New Bcl-2 Inhibitor in Mice. *The Journal of pharmacology and experimental therapeutics* **367:**414-424.

Poulin P and Theil FP (2002a) Prediction of pharmacokinetics prior to in vivo studies. 1. Mechanism-based prediction of volume of distribution. *Journal of pharmaceutical sciences* **91:**129-156.

Poulin P and Theil FP (2002b) Prediction of pharmacokinetics prior to in vivo studies. II. Generic physiologically based pharmacokinetic models of drug disposition. *Journal of pharmaceutical sciences* **91:**1358-1370.

Reed JC (2004) Apoptosis mechanisms: implications for cancer drug discovery. *Oncology (Williston Park)* **18:**11-20.

Rodgers T, Leahy D, and Rowland M (2005a) Physiologically based pharmacokinetic modeling 1: predicting the tissue distribution of moderate-to-strong bases. *Journal of pharmaceutical sciences* **94:**1259-1276.

Rodgers T, Leahy D, and Rowland M (2005b) Tissue distribution of basic drugs: accounting for enantiomeric, compound and regional differences amongst beta-blocking drugs in rat. *Journal of pharmaceutical sciences* **94:**1237-1248.

Rodgers T and Rowland M (2006) Physiologically based pharmacokinetic modelling 2: predicting the tissue distribution of acids, very weak bases, neutrals and zwitterions. *Journal of pharmaceutical sciences* **95:**1238-1257.

Rodgers T and Rowland M (2007) Mechanistic approaches to volume of distribution predictions: understanding the processes. *Pharmaceutical research* **24:**918-933.

Rostami-Hodjegan A, Tamai I, and Pang KS (2012) Physiologically based pharmacokinetic (PBPK) modeling: it is here to stay! *Biopharmaceutics & drug disposition* **33:**47-50.

Rowland M, Benet LZ, and Graham GG (1973) Clearance concepts in pharmacokinetics. *Journal of pharmacokinetics and biopharmaceutics* **1:**123-136.

Sayama H, Komura H, and Kogayu M (2012) Application of hybrid approach based on empirical and physiological concept for predicting pharmacokinetics in humans--usefulness of exponent on prospective evaluation of predictability. *Drug metabolism and disposition: the biological fate of chemicals* **41:**498-507.

Sayama H, Komura H, Kogayu M, and Iwaki M (2013) Development of a hybrid physiologically based pharmacokinetic model with drug-specific scaling factors in rat to improve prediction of human pharmacokinetics. *Journal of pharmaceutical sciences* **102:**4193-4204.

Sekiguchi N, Kato M, Takada M, Watanabe H, Takata S, Mitsui T, Aso Y, and Ishigai M (2011) Quantitative prediction of mechanism-based inhibition caused by mibefradil in rats. *Drug metabolism and disposition: the biological fate of chemicals* **39:**1255-1262.

Sheiner LB and Beal SL (1981) Some suggestions for measuring predictive performance. *Journal of pharmacokinetics and biopharmaceutics* **9:**503-512.

Sun D, Lennernas H, Welage LS, Barnett JL, Landowski CP, Foster D, Fleisher D, Lee KD, and Amidon GL (2002) Comparison of human duodenum and Caco-2 gene expression profiles for 12,000 gene sequences tags and correlation with permeability of 26 drugs. *Pharmaceutical research* **19:**1400-1416.

Tang H and Mayersohn M (2006) A global examination of allometric scaling for predicting human drug clearance and the prediction of large vertical allometry. *Journal of pharmaceutical sciences* **95:**1783-1799.

Wajima T, Yano Y, Fukumura K, and Oguma T (2004) Prediction of human pharmacokinetic profile in animal scale up based on normalizing time course profiles. *Journal of pharmaceutical sciences* **93:**1890-1900.

West GB, Woodruff WH, and Brown JH (2002) Allometric scaling of metabolic rate from molecules and mitochondria to cells and mammals. *Proceedings of the National Academy of Sciences of the United States of America* **99 Suppl 1:**2473-2478.

FOOTNOTES

Emilie Hénin was funded by Fondation Synergie Lyon Cancer and La Ligue Nationale contre le Cancer.

This work is part of a PhD project (Philippe Pierrillas), granted by Servier Laboratories.

François Bouzom is currently working at UCB Biopharma, Development Sciences, Braine l'Alleud, Belgium.

Julien Ogier is currently working at IPSEN Innovation, Translational DMPK & Safety, Les Ulis, France.

Kathryn Ball is currently working at MedImmune, Clinical Pharmacology, Drug Metabolism and Pharmacokinetics, Cambridge, United Kingdom.

Philippe Pierrillas and Emilie Hénin are currently working at Calvagone, Liergues, France.

Legend for Figures

Figure 1: Chemical structure of S 55746.

Figure 2: Observed plasma concentrations versus PBPK plasma concentration predictions in mice, rats, and dogs. Circles represent observations, the dotted line represents the identity line, and the red lines represent the two-fold interval.

Figure 3: AUC and C_{max} in plasma versus doses and day of treatment. Crosses represent the observations, and the blue segments represent the 95% prediction interval of AUC and C_{max}.

DMD Fast Forward. Published on April 2, 2019 as DOI: 10.1124/dmd.118.085605
This article has not been copyedited and formatted. The final version may differ from this version.

TABLES

Table 1: Characteristics of the S 55746 compound

Parameters						
Drug-dependent Parameters						
pKa			Acidic: 9.7 / Base: 6.9			
Log P			4.4			
Molecular weight		$g.mol^{-1}$	710.8			
P_{Caco-2}		10^{-6} cm.s^{-1}	5.00			
Species-dependent Parameters						
			Mouse	*Rat*	*Dog*	*Human*
Unbound fraction in plasma $f_{u,p}$		%	1.50	2.77	1.78	2.50
Blood to plasma ratio $R_{bl:p}$			1.10	1.12	0.81	0.86
In vitro metabolic parameters						
			Mouse	*Rat*	*Dog*	*Human*
Microsome parameters	V_m	pmol/min/mg prot	1310	4260	n/a	1070
	K_m	µM	0.44	1.54	n/a	0.625
Hepatocyte parameters	V_m	pmol/min/10^6 hep	627	n/a	132	283.8
	K_m	µM	3.4	n/a	0.8	1.08
Metabolic pathway in human						
Clearance due to CYP's			85%			
Contribution of CYP's			97% due to CYP3A4			
MBI parameters	k_{inact}	1/h	12.6			
	K_{app}	µM	1.55			
Induction parameters	Ind max		10.41			
	Ind C50	µM	3.03			

DMD Fast Forward. Published on April 2, 2019 as DOI: 10.1124/dmd.118.085605
This article has not been copyedited and formatted. The final version may differ from this version.

Table 2: *In vivo* mouse PK parameters using compartmental PK approach

Parameters (Unit)	Definition	Estimates
V_c (L.kg^{-1})	*Volume of distribution of the central compartment*	1.18
V_p (L.kg^{-1})	*Volume of distribution of the peripheral compartment*	1.15
K_m (ng.ml^{-1})	Drug concentration corresponding to 50% of maximum rate of elimination	654
V_m (mg.h^{-1}.kg^{-1})	Maximum rate of elimination	3.79

DMD Fast Forward. Published on April 2, 2019 as DOI: 10.1124/dmd.118.085605
This article has not been copyedited and formatted. The final version may differ from this version.

Table 3: Prediction performances of the PBPK model in mice

Mouse data			
	AUC		
Dose (mg/kg)	**AUC_{Obs} ($ng.ml^{-1}.h$)**	**AUC_{Pred} ($ng.ml^{-1}.h$)**	**$AUC_{Obs/Pred}$ Ratio**
1	437	311	0.71
3	2020	1256	0.62
10	9170	8032	0.88
25	38846	41616	1.07
	Concentration		
Dose (mg/kg)	**AFE**		**RMSE**
All doses	0.865		0.303
1	0.820		0.138
3	0.672		0.275
10	0.911		0.324
25	1.42		0.491

DMD Fast Forward. Published on April 2, 2019 as DOI: 10.1124/dmd.118.085605
This article has not been copyedited and formatted. The final version may differ from this version.

Table 4: Prediction performance of the PBPK model in rat and dog (model qualification)

Interspecies qualification performance			
	AUC		
Dose (mg/kg)	**AUC_{Obs} ($ng.ml^{-1}.h$)**	**AUC_{Pred} ($ng.ml^{-1}.h$)**	**$AUC_{Obs/Pred}$ Ratio**
	Rat data		
0.5	129	143	1.11
1.5	402	462	1.15
5	1650	1945	1.18
	Dog data		
0.2	110	74	0.67
1.5	908	1236	1.36
	Concentration		
Dose (mg/kg)	**AFE**		**RMSE**
	Rat data		
All doses	0.914		0.195
0.5	0.829		0.156
1.5	0.868		0.133
5	1.04		0.256
	Dog data		
All doses	0.955		0.234
0.2	0.57		0.276
1.5	1.467		0.192

DMD Fast Forward. Published on April 2, 2019 as DOI: 10.1124/dmd.118.085605
This article has not been copyedited and formatted. The final version may differ from this version.

Figures

Figure 1:

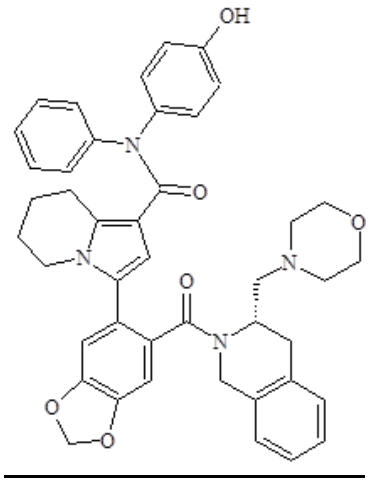

DMD Fast Forward. Published on April 2, 2019 as DOI: 10.1124/dmd.118.085605
This article has not been copyedited and formatted. The final version may differ from this version.

Figure 2:

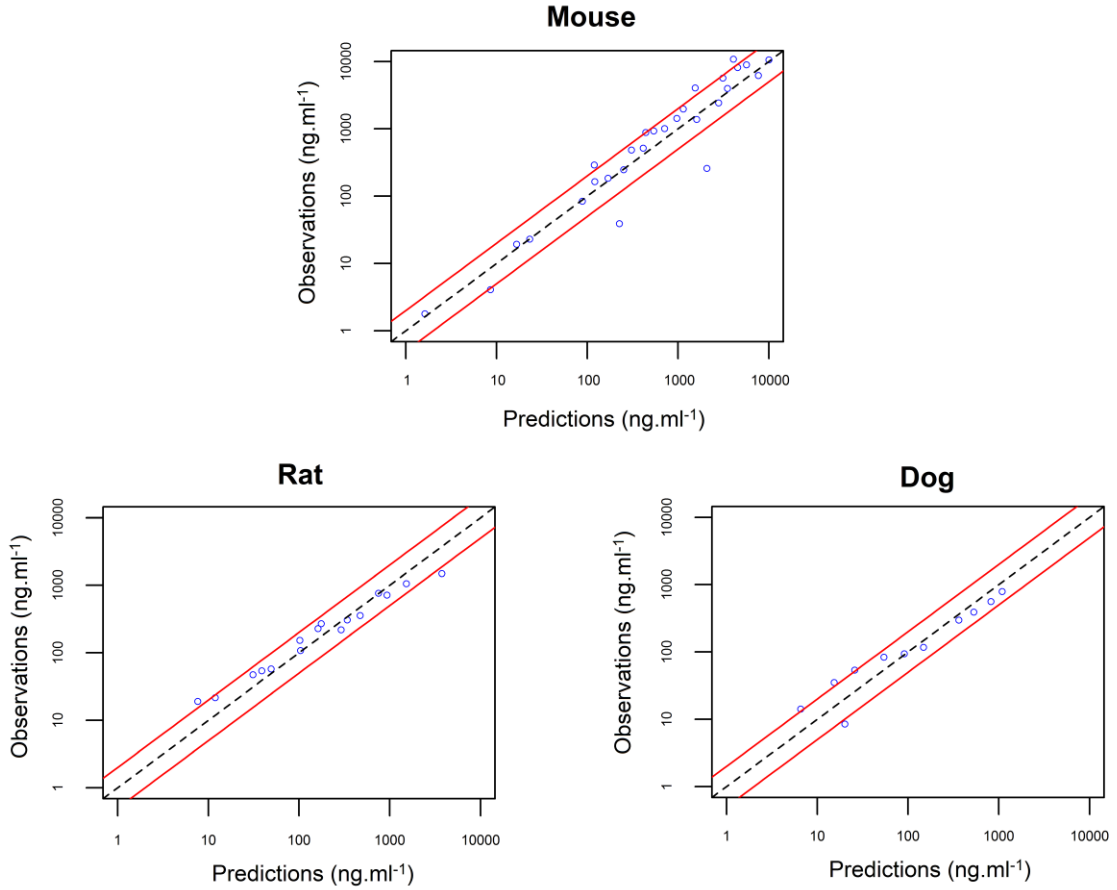

DMD Fast Forward. Published on April 2, 2019 as DOI: 10.1124/dmd.118.085605
This article has not been copyedited and formatted. The final version may differ from this version.

Figure 3:

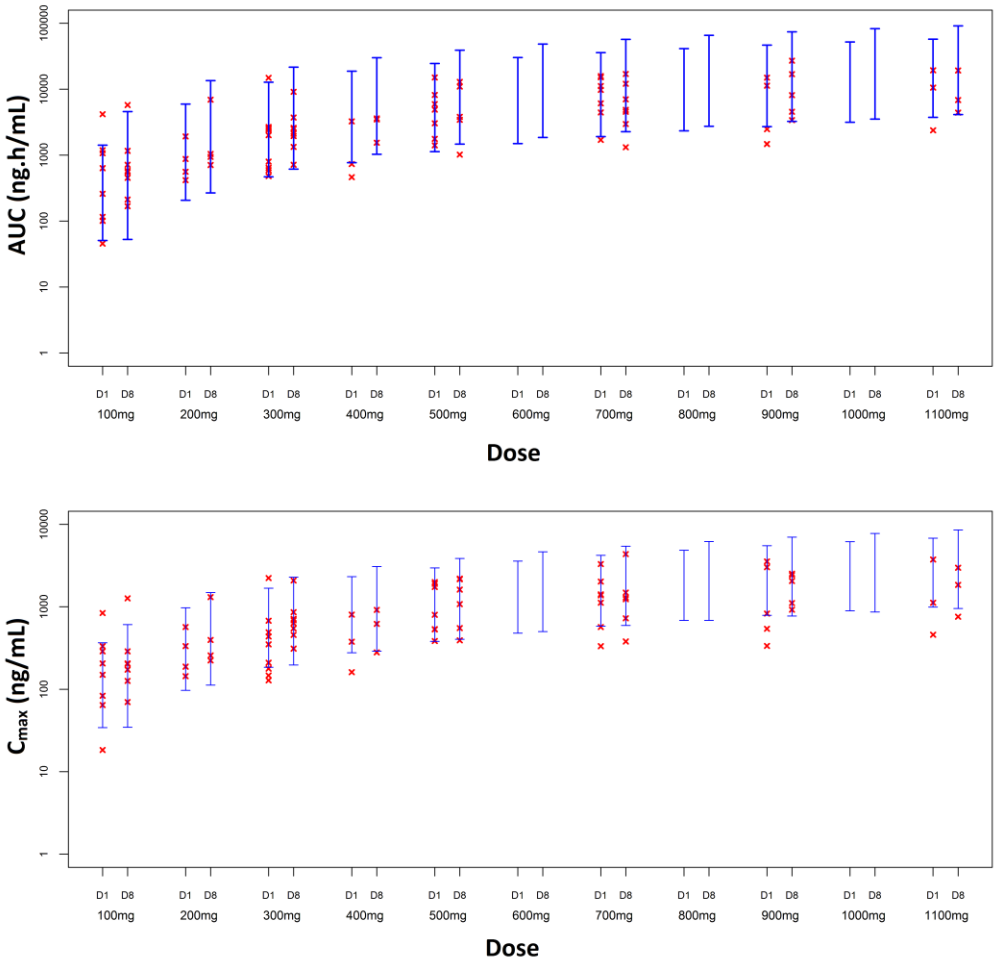

DMD Fast Forward. Published on April 2, 2019 as DOI: 10.1124/dmd.118.085605
This article has not been copyedited and formatted. The final version may differ from this version.

APPENDIX

Appendix 1: Demonstration of the relationship between intrinsic and whole body clearance parameters

We know that:

$$CL_{h,bl} = \frac{Q_h \cdot f_{u,bl} \cdot CL_{int}}{Q_h + f_{u,bl} \cdot CL_{int}} \qquad Eq\ 25$$

In addition,

$$CL_{int} = \frac{V_{m,int}}{K_{m,int} + C_u} \qquad Eq\ 26$$

Therefore, we can write:

$$CL_{h,bl} = \frac{Q_h \cdot f_{u,bl} \cdot V_{m,int}}{K_{m,int} + C_u} \times \frac{K_{m,int} + C_u}{Q_h \cdot (K_{m,int} + C_u) + f_{u,bl} \cdot V_{m,int}} \qquad Eq\ 27$$

$$CL_{h,bl} = Q_h \cdot \left[\frac{f_{u,bl} \cdot V_{m,int}}{(Q_h \cdot K_{m,int} + f_{u,bl} \cdot V_{m,int}) + Q_h \cdot C_u} \right] \qquad Eq\ 28$$

Then,

$$CL_{h,bl} = \frac{f_{u,bl} \cdot V_{m,int}}{\left(K_{m,int} + \frac{f_{u,bl} \cdot V_{m,int}}{Q_h} \right) + C_{bl} \cdot f_{u,bl}} \qquad Eq\ 29$$

$$CL_{h,bl} = \frac{V_{m,int}}{\left[\frac{K_{m,int}}{f_{u,bl}} + \frac{V_{m,int}}{Q_h} \right] + C_{bl}} \qquad Eq\ 30$$

Moreover,

$$CL_{h,bl} = \frac{V_m}{K_m + C_{bl}} \qquad Eq\ 31$$

Which permits us to write:

$$\frac{V_m}{K_m + C_{bl}} = \frac{V_{m,int}}{\left[\frac{K_{m,int}}{f_{u,bl}} + \frac{V_{m,int}}{Q_h} \right] + C_{bl}} \qquad Eq\ 32$$

And from this equation we can deduce:

$$\begin{cases} V_m = V_{m,int} & Eq\ 33 \\ K_m = \left[\frac{K_{m,int}}{f_{u,bl}} + \frac{V_{m,int}}{Q_h} \right] & Eq\ 34 \end{cases}$$